Outline

- Watanabe et al., JCE, 2001
- Echebarria and Karma, PRL, 2002; Condmat 2006 (50 pages)
- Echebarria and Karma, Chaos 2002
- Christini et al., PRL 2006
- Shiferaw et al., Biophys J, 2003
- Shiferaw et al., Phys. Rev. E, 2005
- Shiferaw and Karma, PNAS, 2006
- Sato et al., Circ. Res. 2006 (submitted)

Discordant Sand Alternans
Swinney et al., 1995

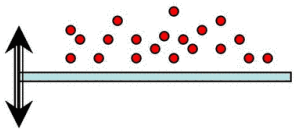

$$z = \mathrm{A}\cos 2\pi f\ \mathrm{t}$$

A single sand grain can be driven into alternans by a vibrating platform

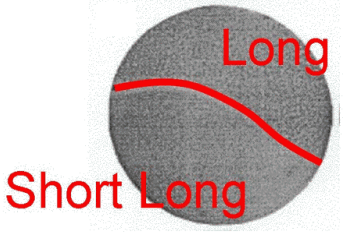

Many sand grains can exhibit discordant alternans

Discordant Alternans

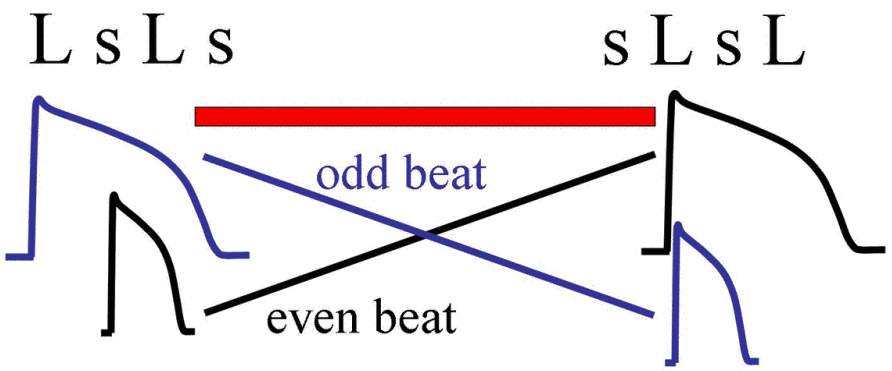

Discordant Alternans → Spatial gradient of repolarization → Reentry VT/VF

Gradient> 10 msec/mm

Discordant Alternans →VF

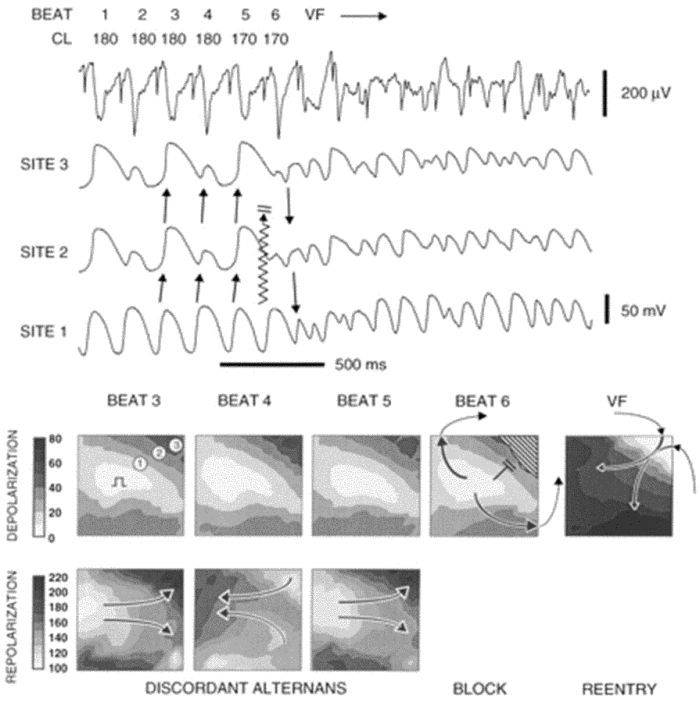

Pastore et al., 1999

Are spatially discordant tissue scale electrical alternans of static or dynamic origin ?

Discordant alternans =
spatially out-of-phase period doubling oscillations

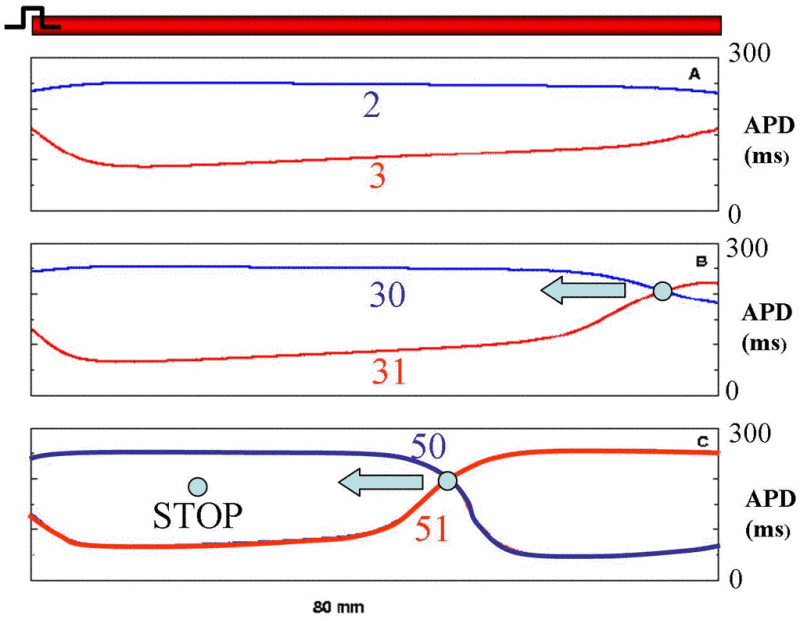

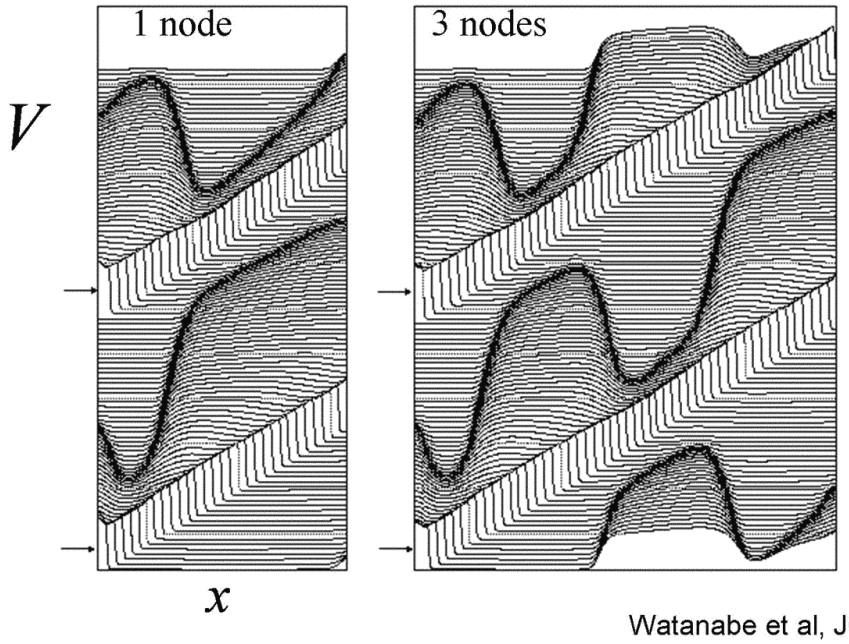

Watanabe et al, JCE 2001

Surprise: wave patterns ?

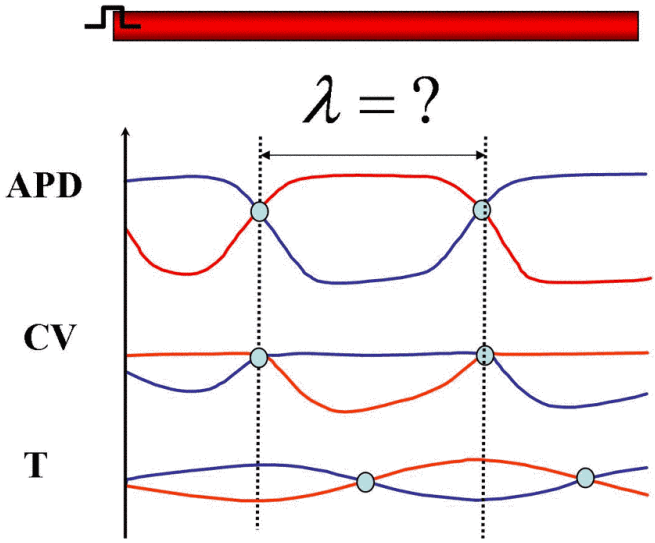

Both standing and travelling waves are possible.

How do these wave patterns form and what determines their wavelength ?

Alternans

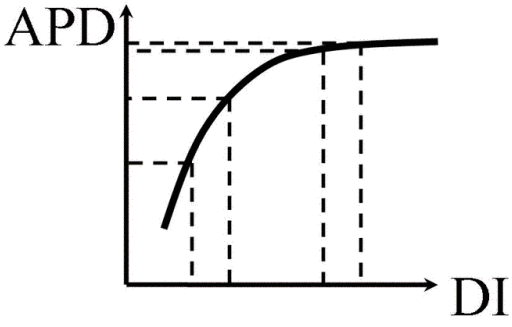

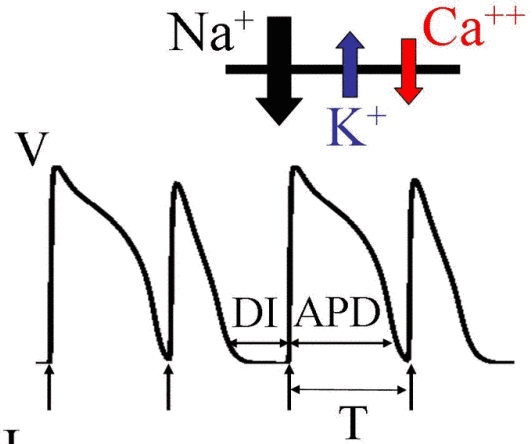

$$APD^{n} = f(T - APD^{n-1})$$

Steep slope of APD-restitution + constant T → Alternans

L s L s L s ….

Dephasing

L s L s → s L s L

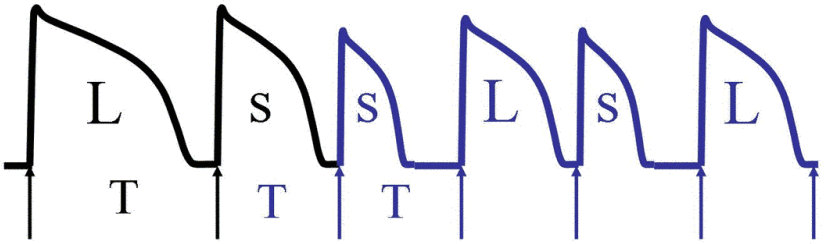

Change of T ➡ Change of phase

$T < T^*$

CV-Restitution

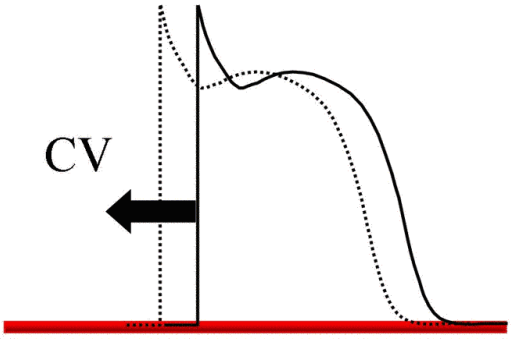

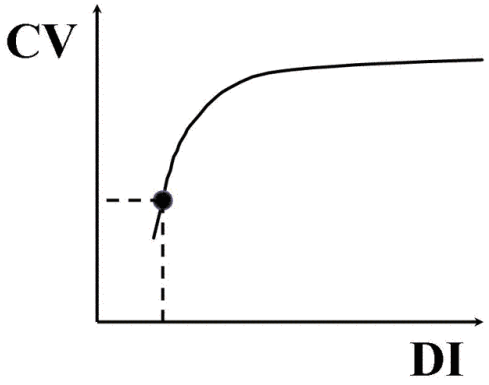

The instantaneous speed of the activation wavefront, or conduction velocity (CV), depends on the local diastolic DI, and thus on position along the cable.

Nonlocal Dephasing

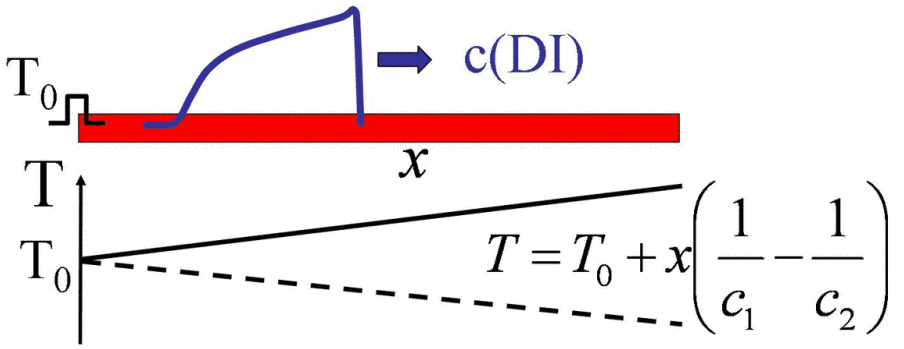

Conduction restitution → Gradient of T → Dephase

Mechanisms of Discordance

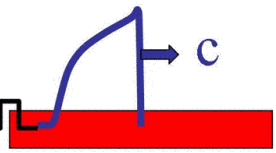

- Conduction restitution
  (Qu et al, 2000; Watanabe et al, 2001; Echebarria-Karma, 2002)
- Ectopic beat 
  (Watanabe et al, 2000)
- Heterogeneous APD-restitution
  (Echebarria-Karma, 2002) 

Extension to tissue of spatially coupled maps of Courtemanche, Glass and Keener (1993)

$$D^n(x) = T^n(x) - f(D^{n-1}(x))$$

$$T^n(x) = t_{n+1} - t_n$$

$$= T_0 + \int_0^x \frac{dx'}{c(D^n(x'))} - \int_0^x \frac{dx'}{c(D^{n-1}(x'))}$$

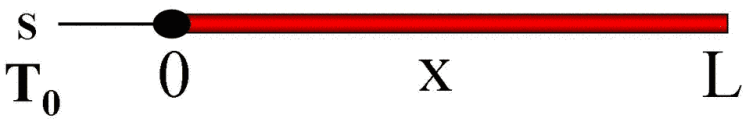

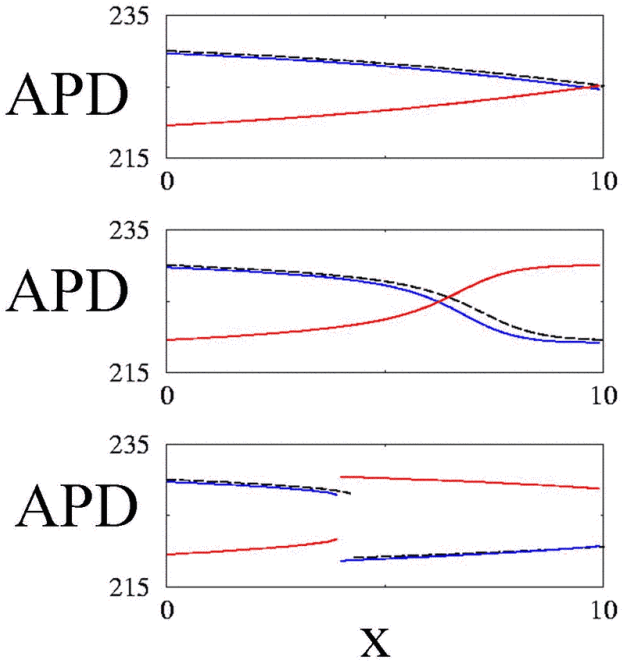

$$APD^n = APD_c + a\,(-1)^n$$

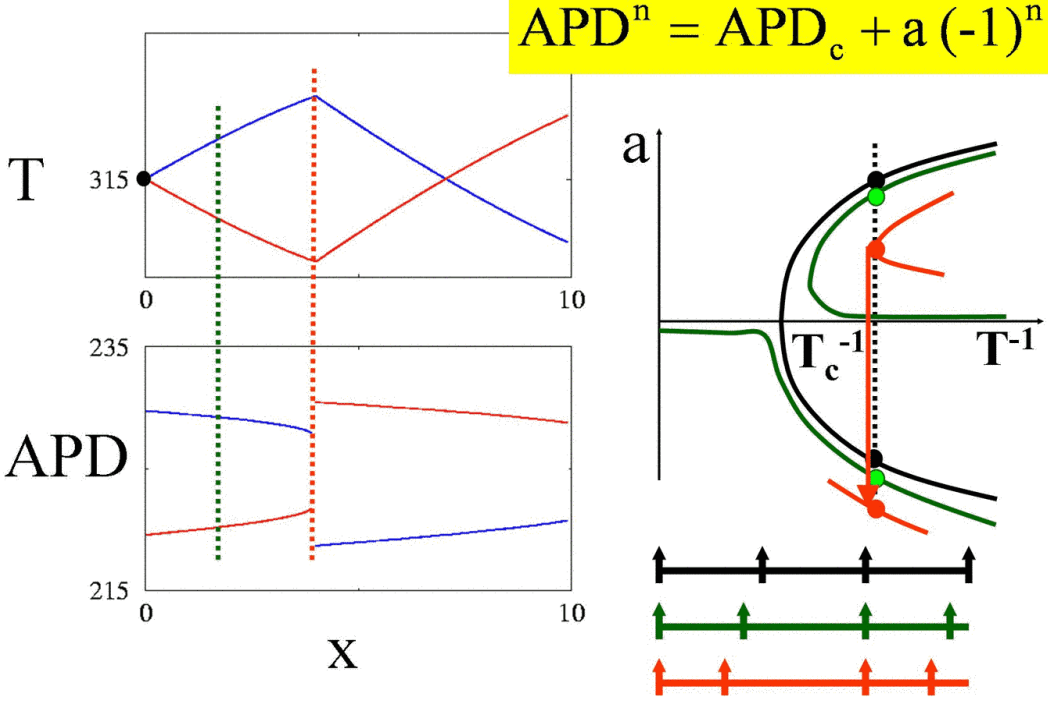

Echebarria-Karma, PRL **88**, 208101 (2002)

$$APD^n \approx APD_c + a\, e^{i\pi n}$$

$$T^n \approx T_c + b\, e^{i\pi n}$$

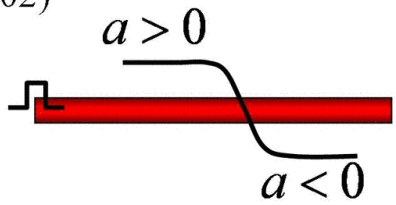

$$\partial_t a = \sigma\, a - \chi\, a^3 + \xi^2\, \partial_x{}^2 a - w\, \partial_x a - b$$

$$b(x) = b(0) + \frac{1}{\Lambda}\int_0^x dx'\, a(x')$$

$$\xi \sim \left(D \times APD_c\right)^{1/2} \qquad w \sim D/c \qquad \Lambda = \frac{c^2}{2c'}$$

Linear stability

$$a \sim \exp(ikx + \Omega t)$$

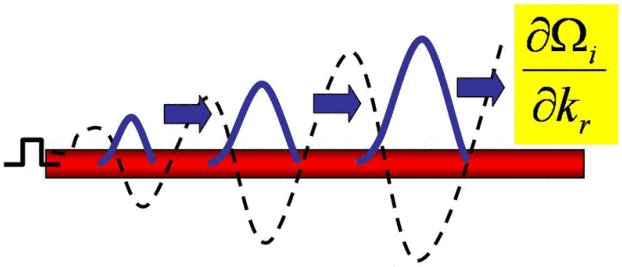

$$\partial_t a = \sigma\, a - \frac{1}{\Lambda}\int_0^\infty dx'\, a(x') - w\, \partial_x a + \xi^2\, \partial_x{}^2 a$$

$$\Omega = \sigma - \xi^2 k^2 - i\left(wk - \frac{1}{\Lambda k}\right)$$

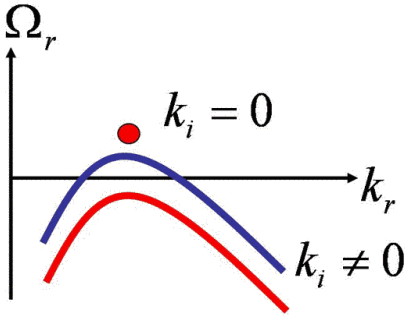

$$\lambda_{stationary} \sim (w\Lambda)^{1/2}$$

$$\lambda_{traveling} \sim (\xi^2\Lambda)^{1/3}$$

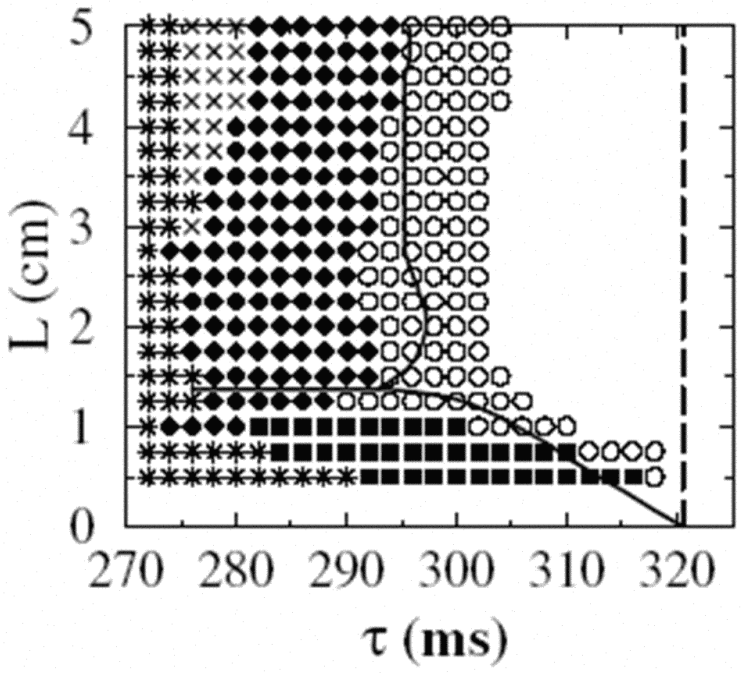

$$\lambda_{stationary} = 2\pi(w\Lambda)^{1/2}$$

TABLE I. Values of various lengths in cm with λ_{theor} [Eqs. (12) or (13)] and λ_{sim} [from simulations of Eq. (7)].

Model	Λ	w	ξ	$\lambda_{theor}/4$	$\lambda_{sim}/4$	L_{min}
Noble	49.1	0.045	0.18	2.33	2.6	2.75
Two-variable	3.55	0.031	0.235	1.33	1.1	1.15

$$w \sim D/c \qquad \Lambda = \frac{c^2}{2c'}$$

Conclusion

Period doubling
+ nonlocal dephasing
+ advection and diffusion

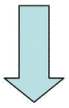

Spatial patterns via finite k instability
stationary (advection dominated)
convective (diffusion dominated)

Control

$$T^n = T_0 + \frac{\gamma}{2}(APD^n - APD^{n-1})$$

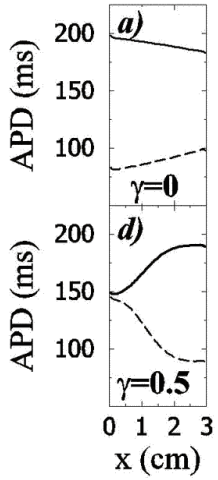

Echebarria-Karma (2002)

$$a(x,t) = \psi(x)e^{\Omega t}$$

Forced Helmholtz equation

$$\xi^2 \frac{d^2\psi}{dx^2} + (\sigma - \Omega)\psi = \gamma\psi(0)$$

$$\Omega_0 = \sigma - \gamma$$

$$\Omega_n = \sigma - \frac{n^2\pi^2\xi^2}{L^2}$$

$$\psi_n \sim 1 + \left(\frac{n^2\pi^2\xi^2}{\gamma L^2} - 1\right)\cos\frac{n\pi x}{L}$$

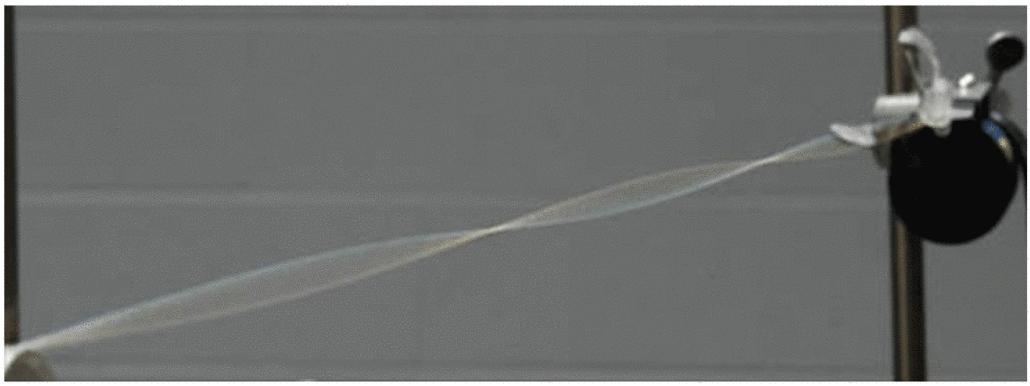

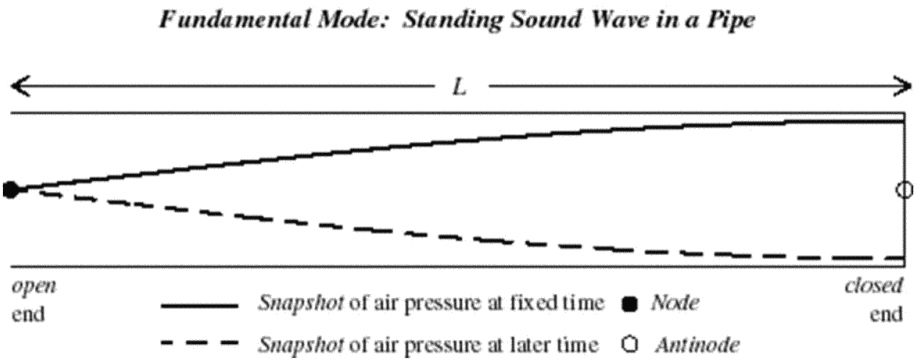
Fundamental Mode: Standing Sound Wave in a Pipe
L
open end
closed end
Snapshot of air pressure at fixed time
Node
Snapshot of air pressure at later time
Antinode

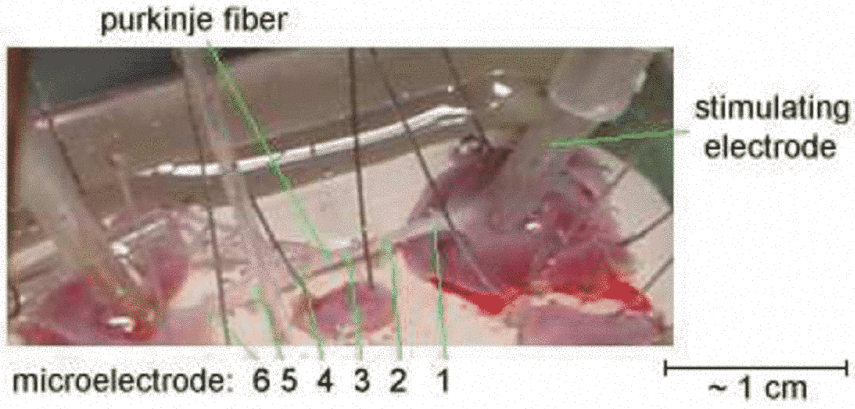
purkinje fiber
stimulating electrode
microelectrode: 6 5 4 3 2 1
~ 1 cm

$$a(x) \approx \frac{a(L)}{2}\left[1 - \cos\frac{\pi x}{L}\right]$$

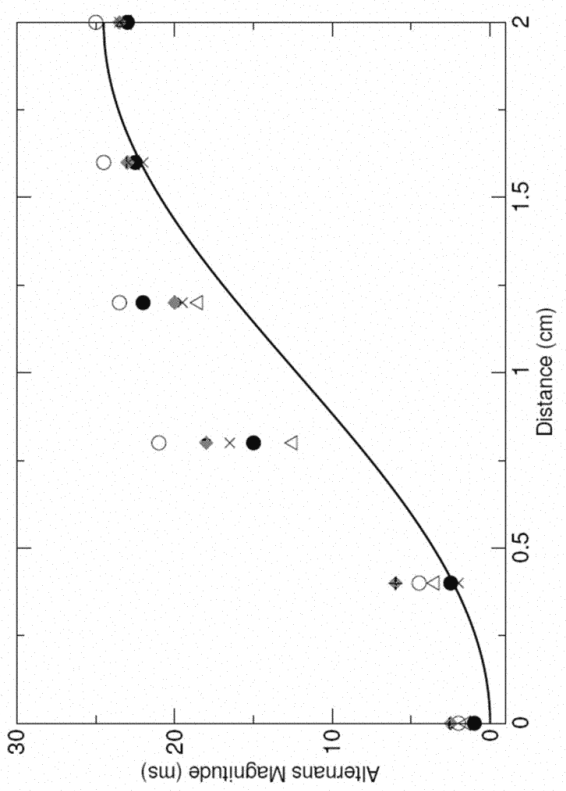

EC coupling

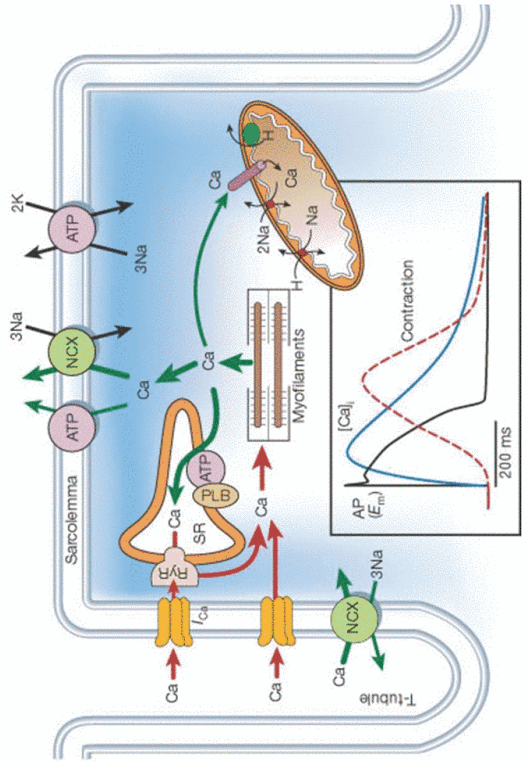

Who is the master and who is the slave???

Chudin *et al.* (2003)

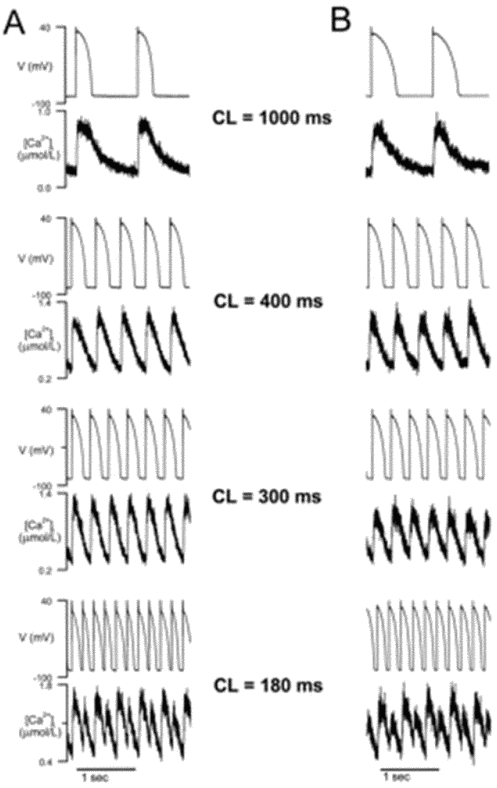

Subcellular discordant alternans

Blatter *et al.* (2003)

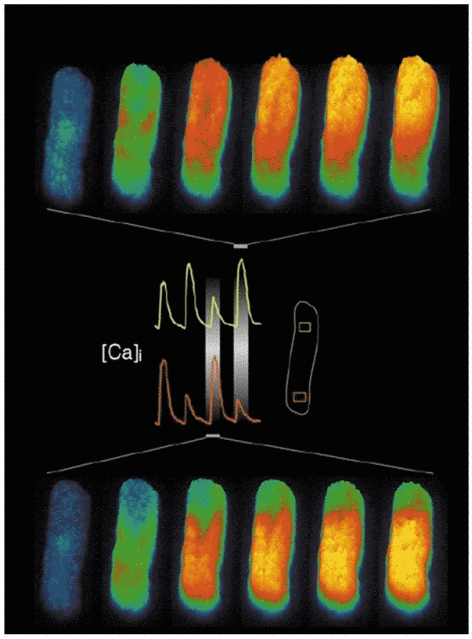

Complex APD-Ca_i Behavior in the Single Myocyte

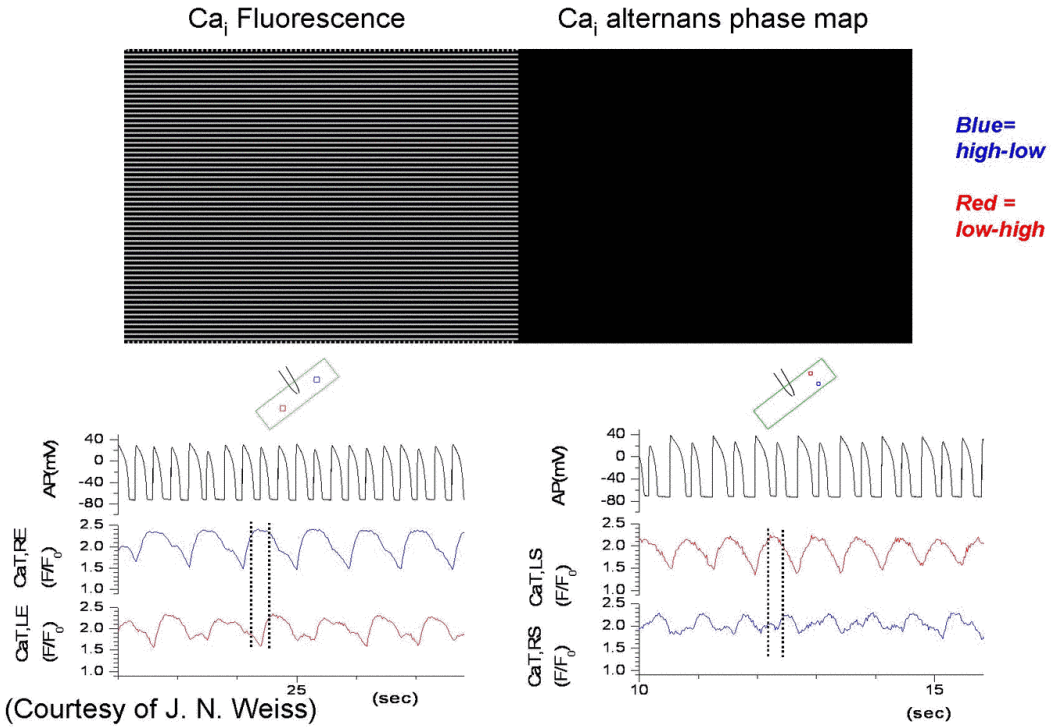

(Courtesy of J. N. Weiss)

Rabbit ventricular myocyte, perforated patch, 23^{0}C (Experiment by Lai-Hua Xie, PhD)

Are spatially discordant subcellular scale calcium alternans of static or dynamic origin ?

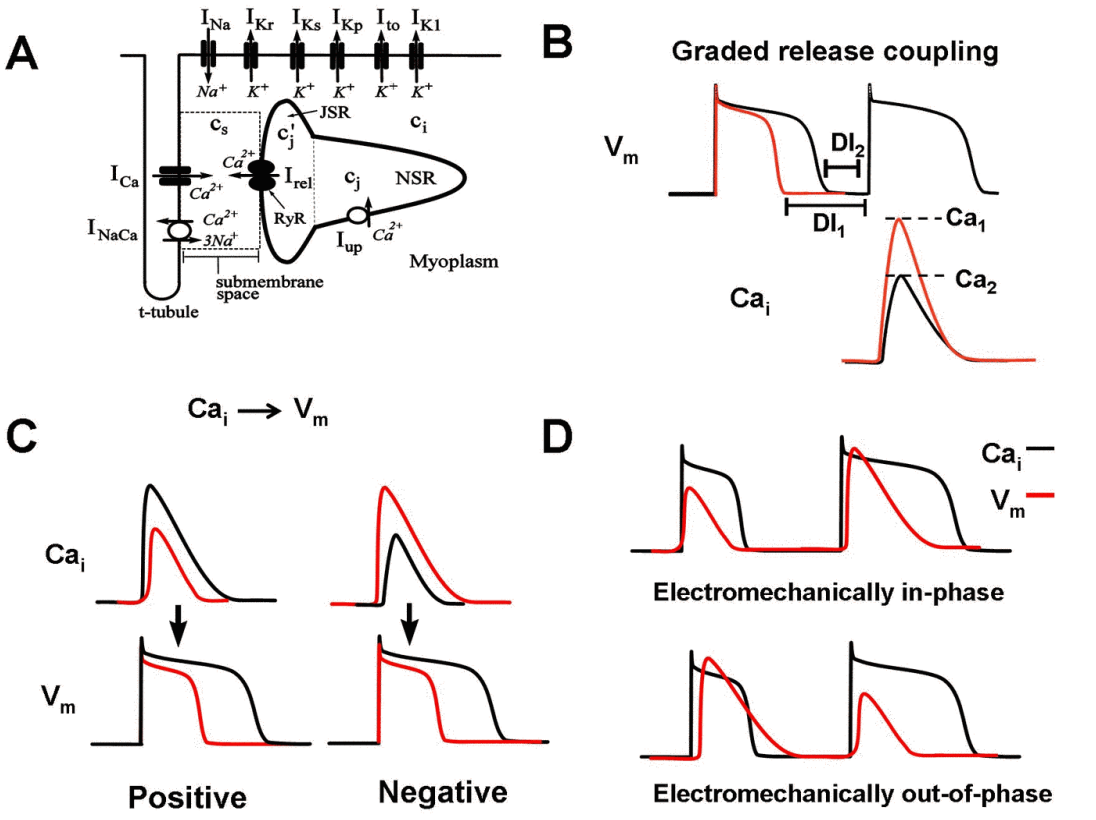
A
I_{Na} I_{Kr} I_{Ks} I_{Kp} I_{to} I_{K1}
Na^+ K^+ K^+ K^+ K^+ K^+
JSR
c_s
c_j'
c_i
I_{Ca}
Ca^{2+}
I_{rel}
c_j
NSR
I_{NaCa}
$3Na^+$
RyR
I_{up}
Myoplasm
submembrane space
t-tubule
B
Graded release coupling
V_m
DI_2
DI_1
Ca_1
Ca_2
Ca_i
C
$Ca_i \rightarrow V_m$
Ca_i
V_m
Positive
Negative
D
Ca_i
V_m
Electromechanically in-phase
Electromechanically out-of-phase

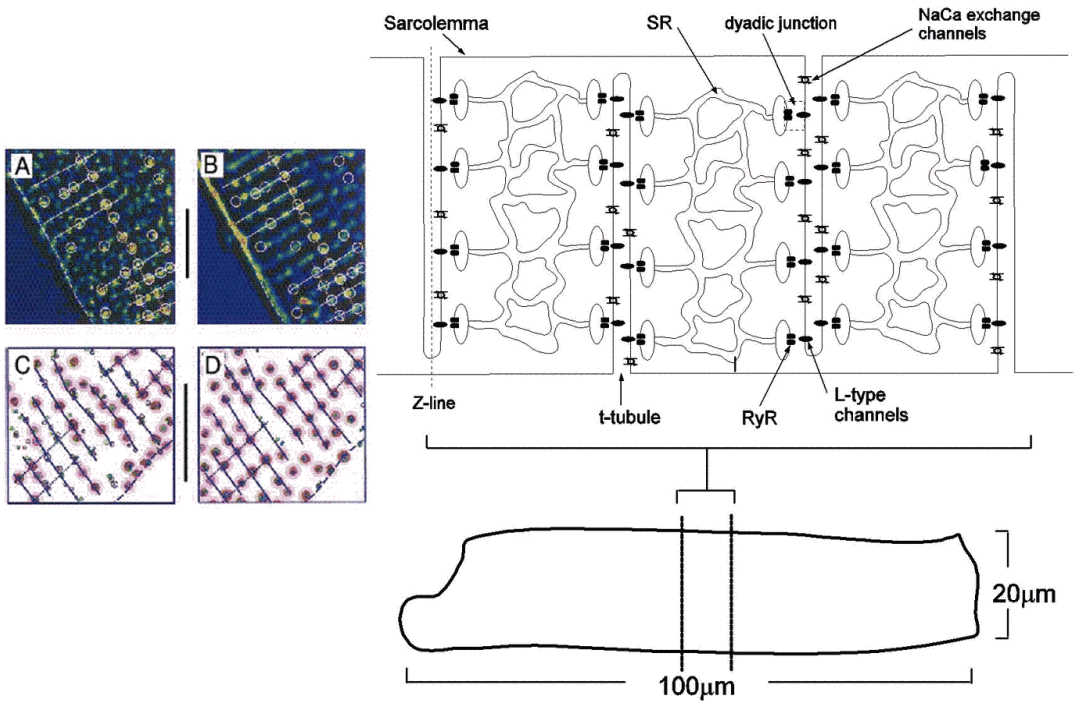
A
B
C
D
Sarcolemma
SR
dyadic junction
NaCa exchange channels
Z-line
t-tubule
RyR
L-type channels
20μm
100μm

Results & interpretation

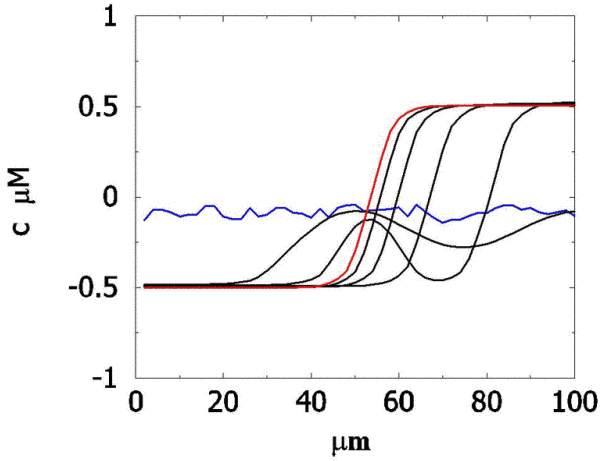

Shiferaw & Karma, PNAS (2006)

$$APD^n = APD^* - a\,(-1)^n$$

$$Ca_i^n = Ca_i^* + c\,(-1)^n$$

Turing-like instability

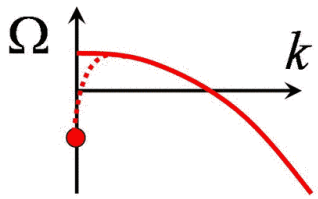

$$\partial_t a = \alpha\, a + \beta\, \bar{c}$$

$$\partial_t c = \gamma\, a + \delta\, c + \mu\, \bar{c} + D\nabla^2 c$$

Desynchronization mechanism

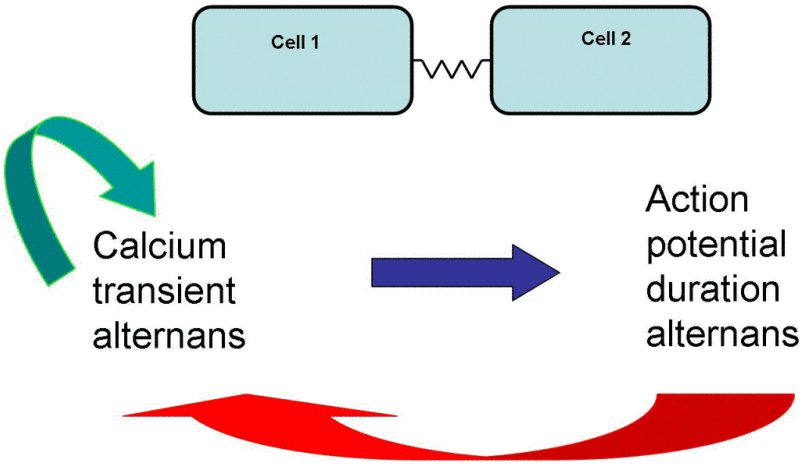

Conclusion

Turing-like instability mediated by calcium (activator) and voltage (inhibitor) diffusion leads to subcellular patterns of spatially discordant calcium alternans.

What are the tissue scale manifestations of desynchronization ?

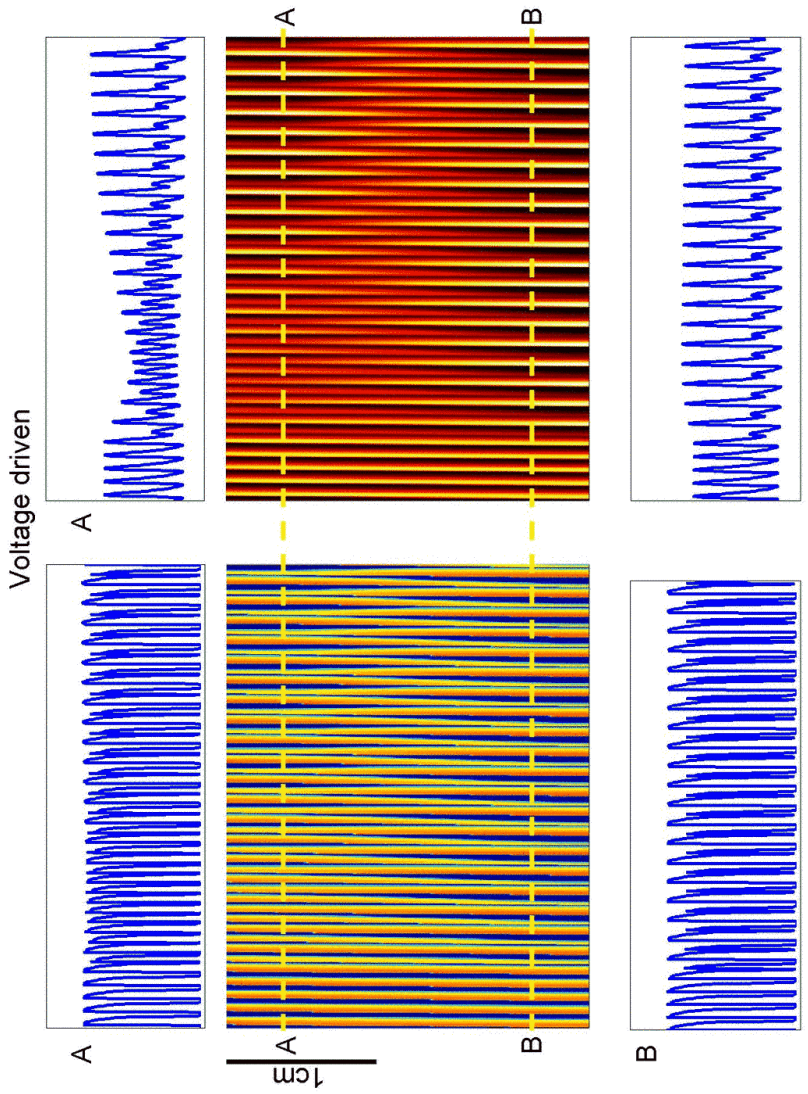
Voltage driven
A
A
A
B
B
B
1cm

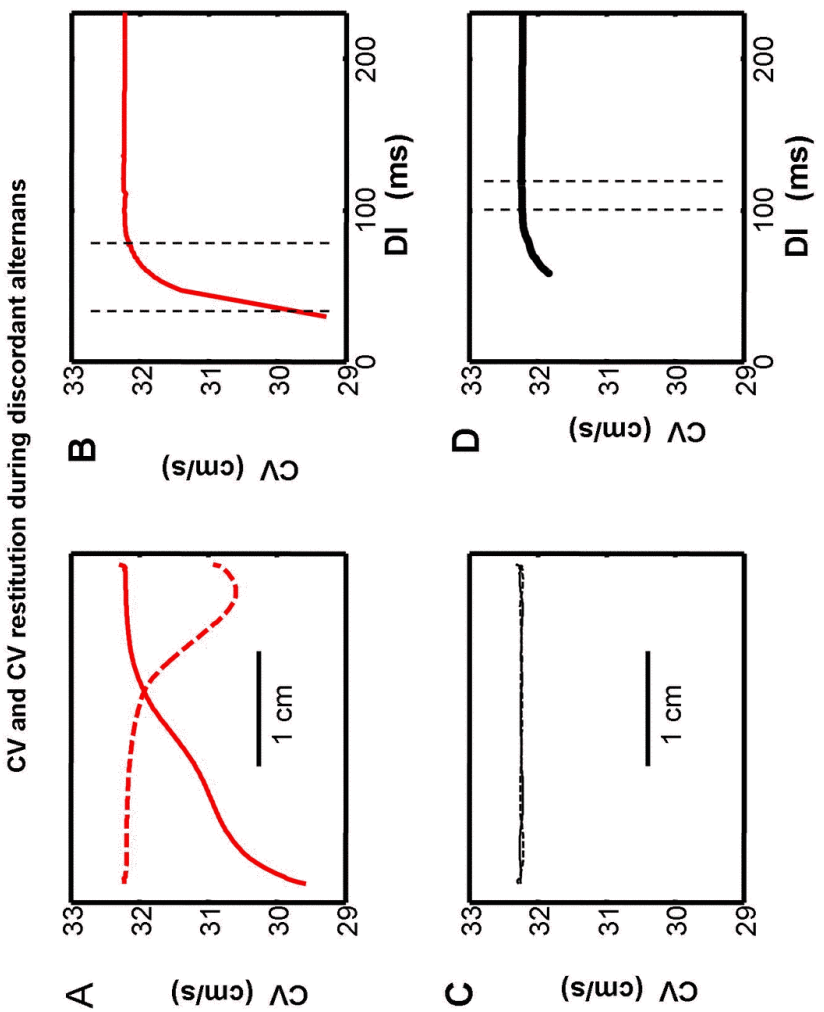
CV and CV restitution during discordant alternans
A
B
C
D
CV (cm/s)
DI (ms)
1 cm
33
32
31
30
29
0
100
200

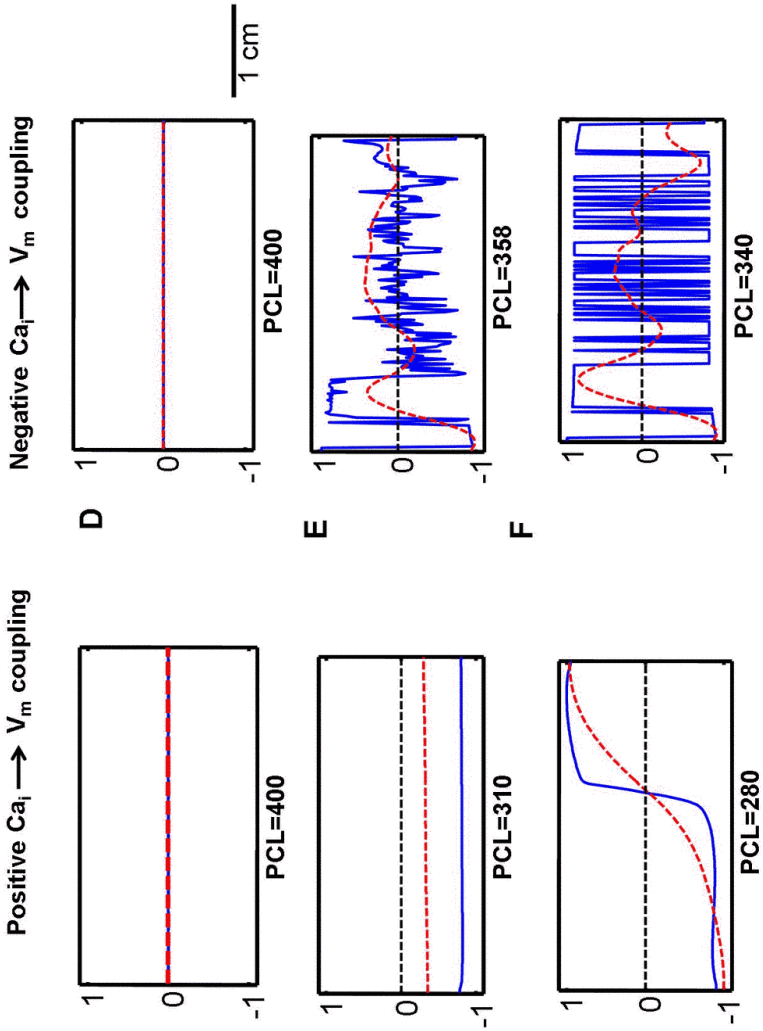
Positive Ca$_i$ → V$_m$ coupling
Negative Ca$_i$ → V$_m$ coupling
A
B
C
D
E
F
PCL=400
PCL=310
PCL=280
PCL=400
PCL=358
PCL=340
1 cm

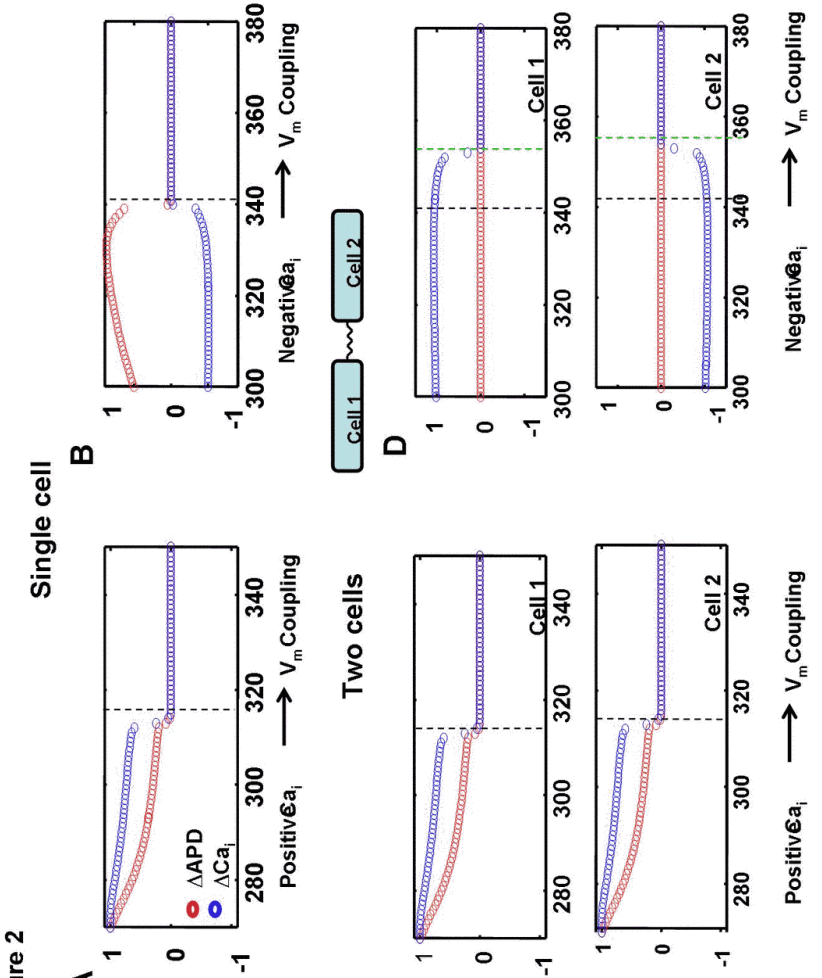
Single cell
Two cells
A
B
C
D
ΔAPD
ΔCa$_i$
Positive Ca$_i$ → V$_m$ Coupling
Negative Ca$_i$ → V$_m$ Coupling
Cell 1
Cell 2

Figure 2

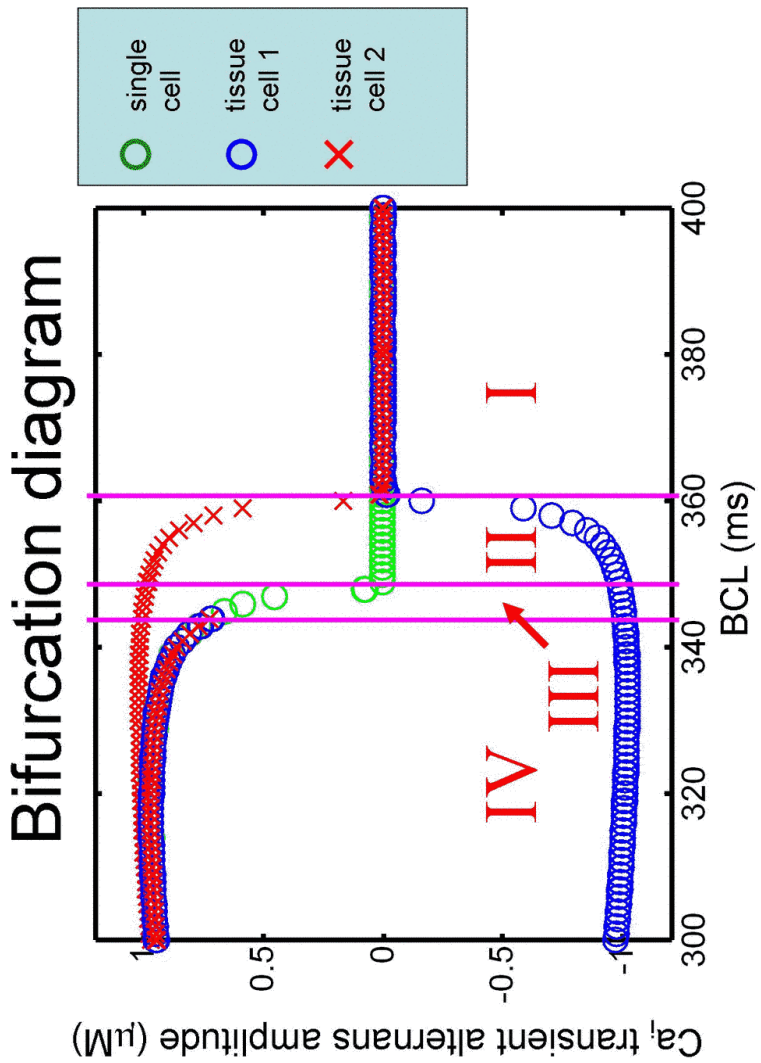
Bifurcation diagram
single cell
tissue cell 1
tissue cell 2
I
II
III
IV
BCL (ms)
300
320
340
360
380
400
1
0.5
0
-0.5
-1
Ca_i transient alternans amplitude (μM)

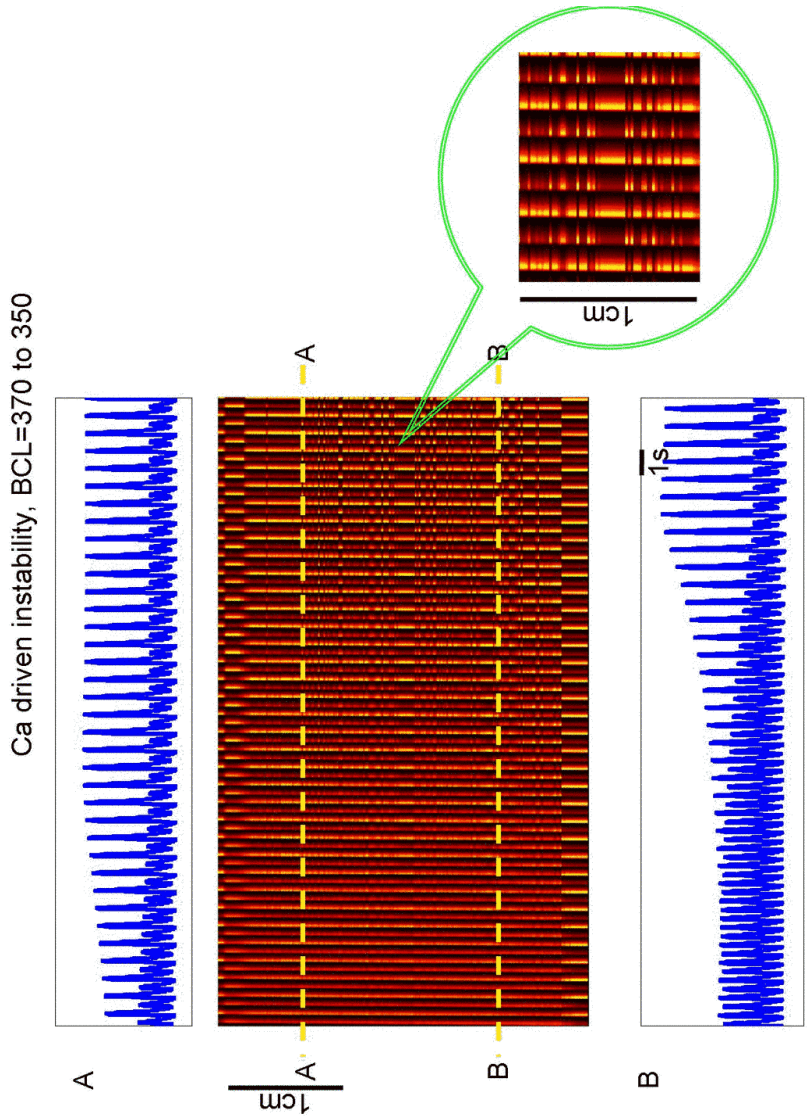
Ca driven instability, BCL=370 to 350
A
B
1cm
1s

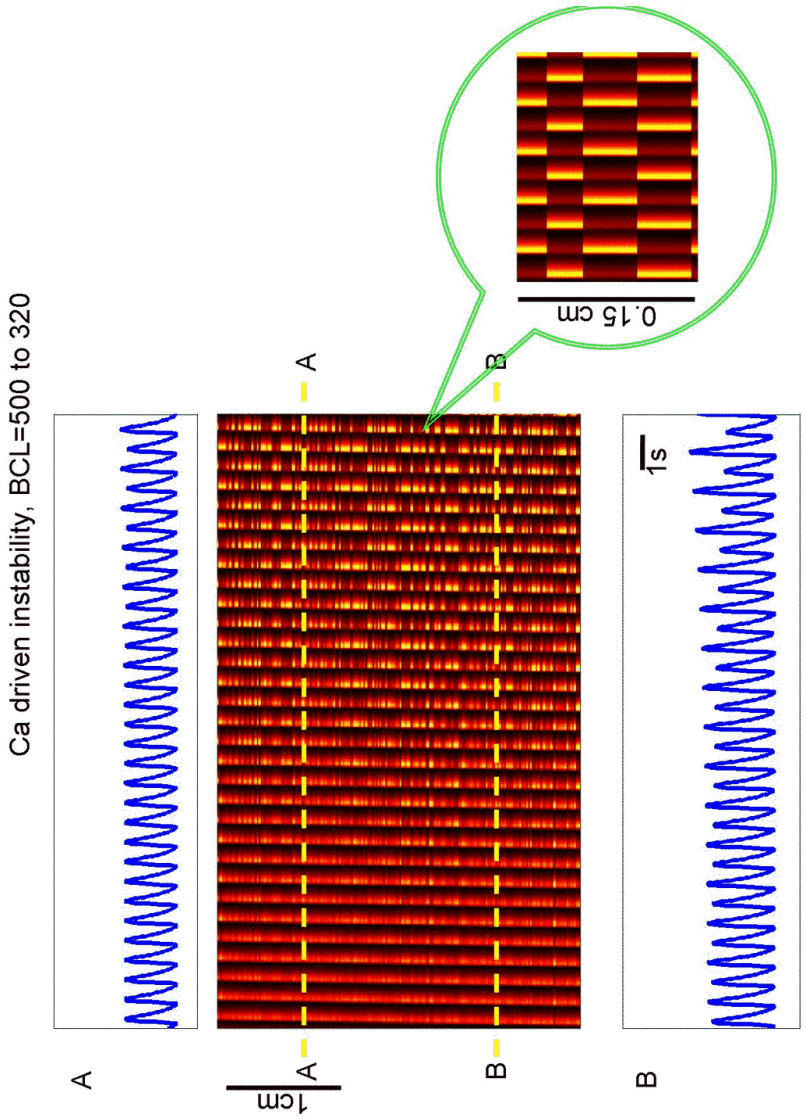
Ca driven instability, BCL=500 to 320
A
B
0.15 cm
1s
A
1cm
A
B
B

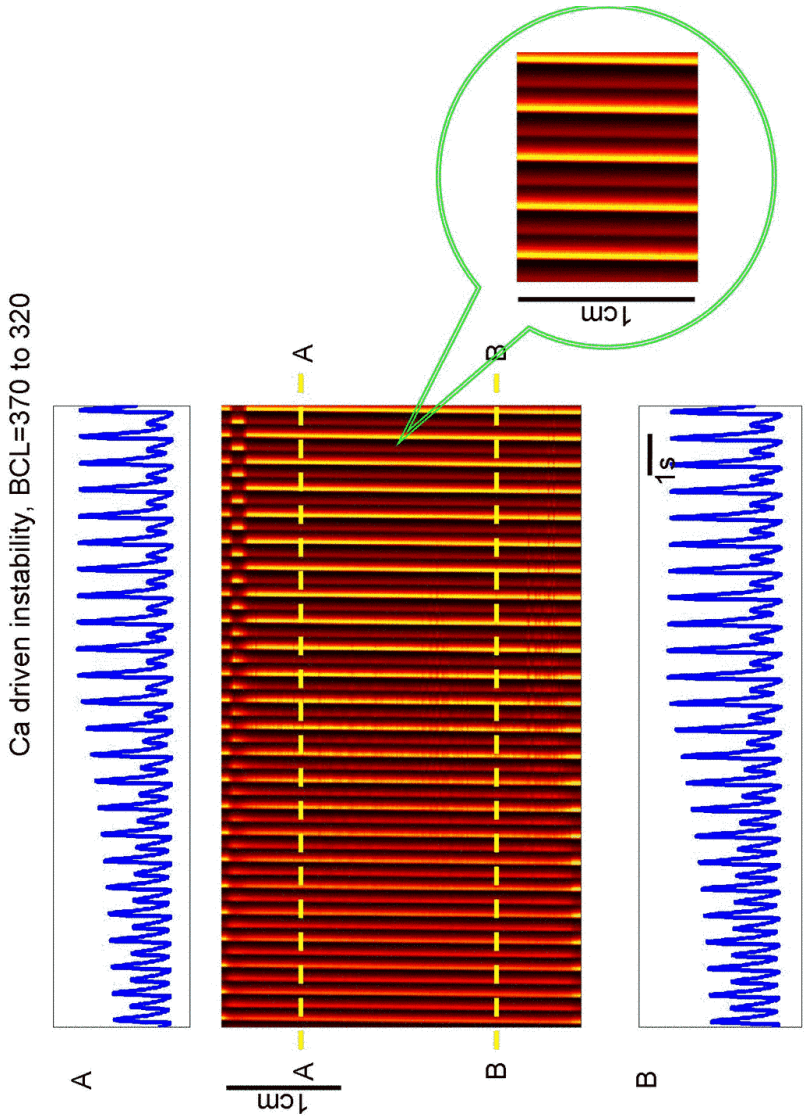
Ca driven instability, BCL=370 to 320
A
B
1cm
1s
A
1cm
A
B
B

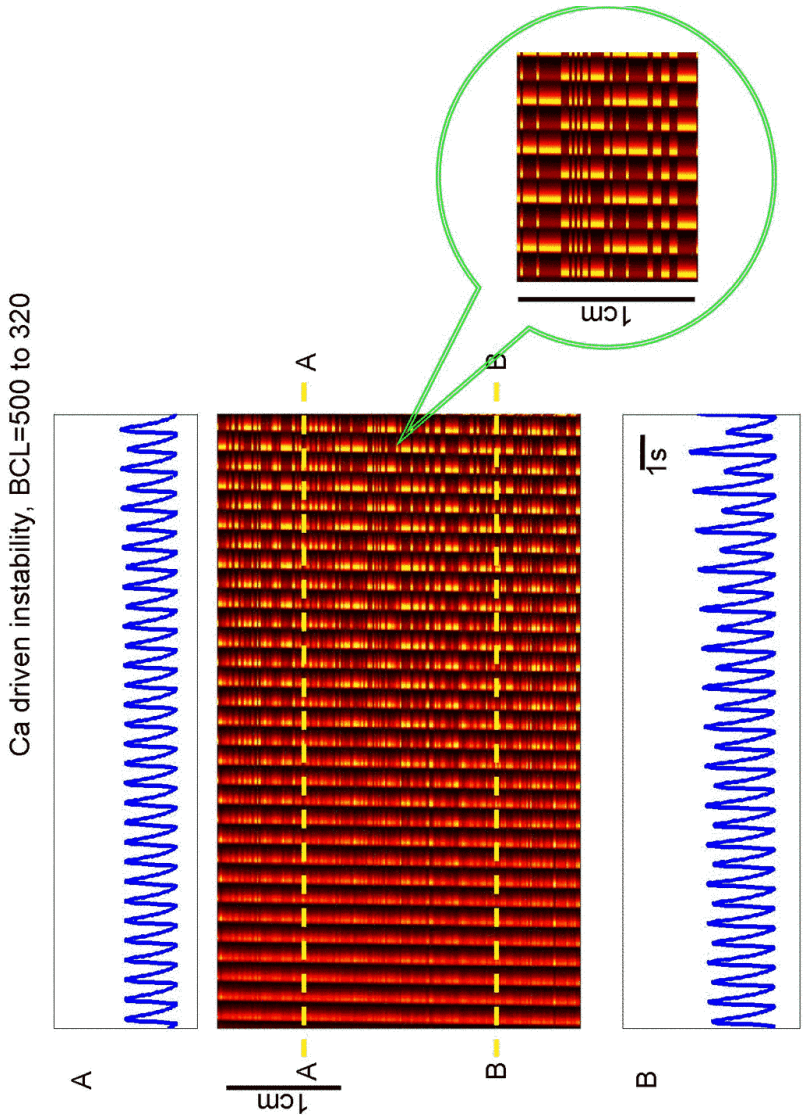
Ca driven instability, BCL=500 to 320
A
B
1cm
1s
A
B
1cm

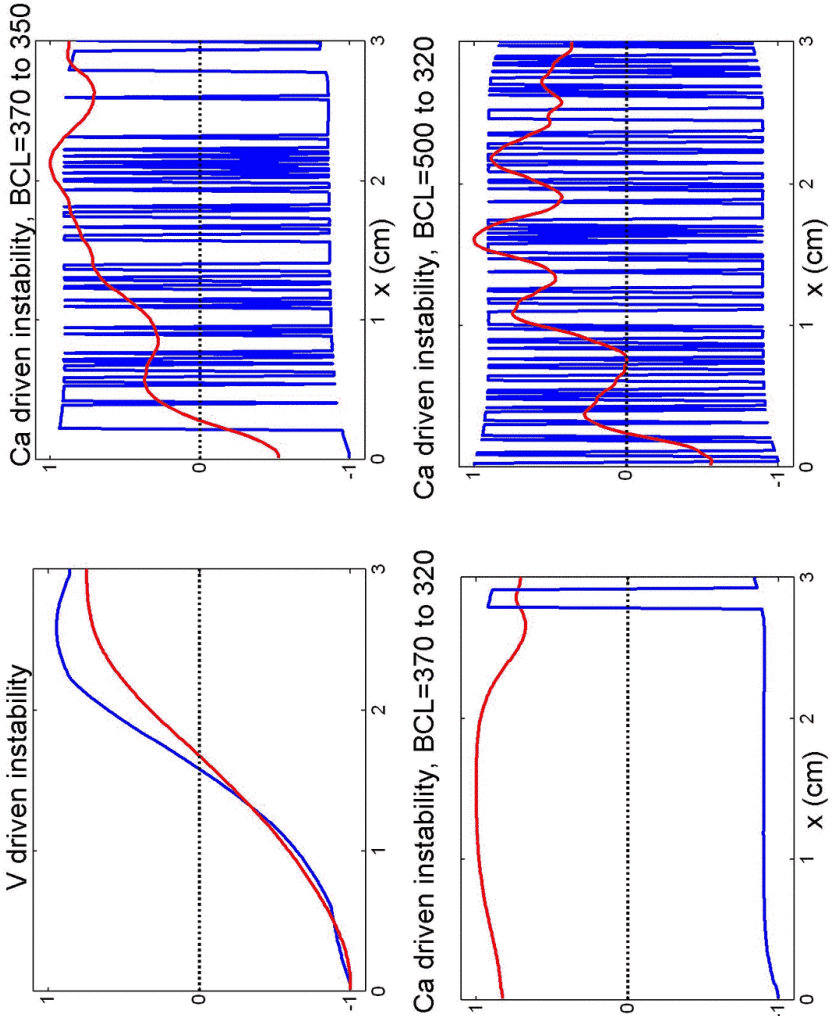
Ca driven instability, BCL=370 to 350
Ca driven instability, BCL=500 to 320
V driven instability
Ca driven instability, BCL=370 to 320
x (cm)
x (cm)
x (cm)
x (cm)

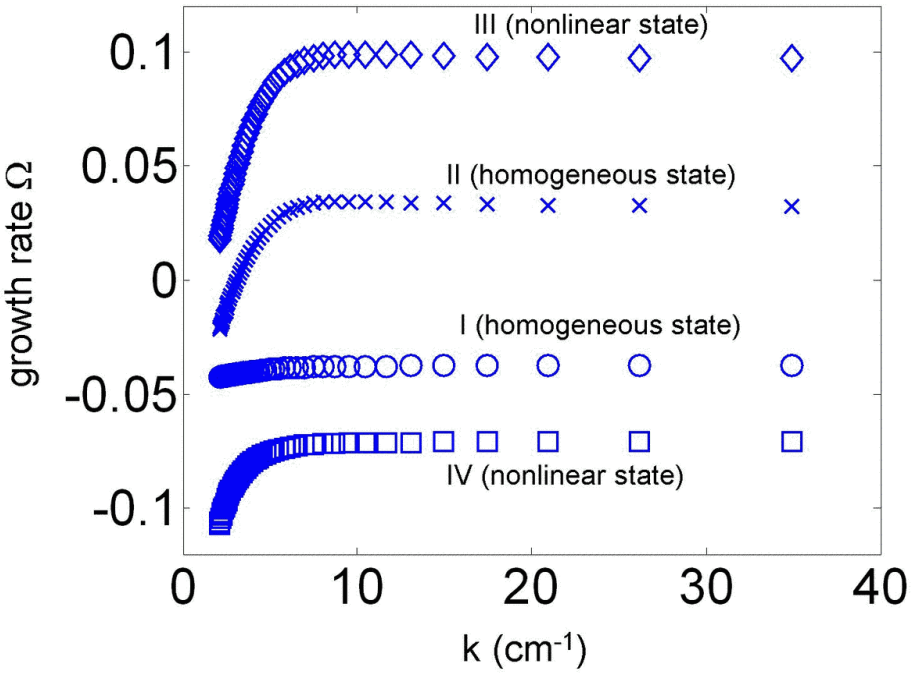

Conclusion

- Patterns of alternans influenced by both sign of coupling and initial conditions
- Spatial scale of nodal region related to cellular mechanism of alternans

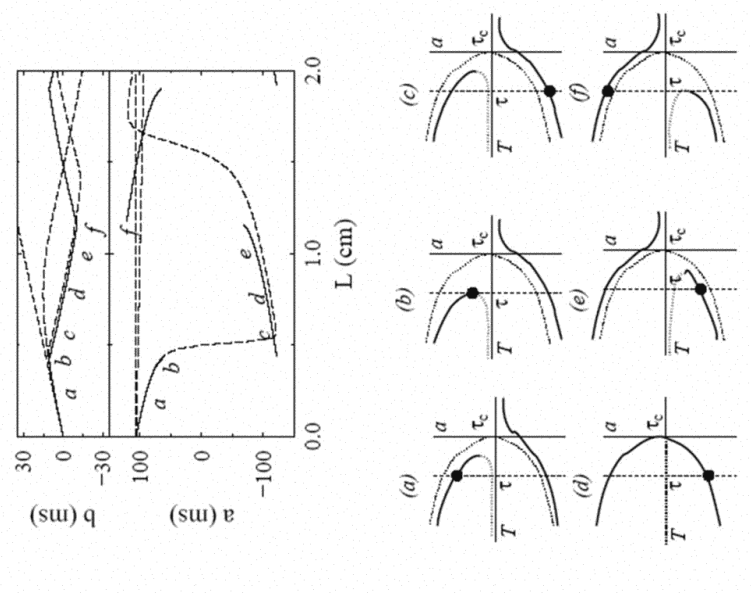
b (ms)
a (ms)
L (cm)
0.0
1.0
2.0
30
0
−30
100
0
−100
a
b
c
d
e
f
(a)
(b)
(c)
(d)
(e)
(f)
τ_c
τ
T